EURASIAN PHYSICAL TECHNICAL JOURNAL

2025, Volume 22, No. 4 (54)

https://doi.org/10.31489/2025N4/5-23

Received: 06/09/2025 Revised: 14/11/2025 Accepted: 20/12/2025 Published online: 29/12/2025

Research Article

UDC 539.199, 544.723.2

CONFORMATIONAL STRUCTURE OF BINARY POLYPEPTIDE COMPLEXES ON THE SURFACE OF A CHARGED GOLD NANOPARTICLE WITH CHANGING PH

Kruchinin N.Yu.*, Kucherenko M.G.

Center of Laser and Informational Biophysics, Orenburg State University, Orenburg, Russia
*Corresponding author: kruchinin_56@mail.ru

Abstract. *Using molecular dynamics simulation, pH-sensitive conformations of binary complexes of homogeneous polypeptides located on the surface of a charged spherical gold nanoparticle were studied. A mathematical model of conformations has been developed taking into account interactions in a complex of two homogeneous polymers on the surface of a charged spherical nanoobject. When two polypeptides were adsorbed on a nanoparticle, the structure of the macromolecular corona depended significantly on the polypeptide combinations in the binary complex. Two identical homogeneous polypeptides shifted away from each other along the neutral surface when their pH deviated from the isoelectric point, while on the surface of a similarly charged nanoparticle, the macrochain corona became strongly loosened. On the charged nanoparticle, the polymer shell of the two polypeptides of opposite polarities delaminated, and the shell itself swelled significantly. When one of the polypeptides in this binary complex reached the isoelectric point, the second charged polypeptide unfolded and disengaged from the first macrochain, shifting away from the surface of the similarly charged nanoparticle.*

Keywords: polypeptide complex, molecular dynamics simulation, conformational transformations, charged nanoobject.

1. Introduction

Currently, shell nanosystems have found wide application in drug delivery [1], as elements in various sensors, such as sensors based on surface-enhanced Raman scattering (SERS) [2], surface plasmon resonance (SPR) [3] and Förster resonance energy transfer (FRET) [4]. Of great interest in biochemistry and biomedicine is the creation of such sensors, nanoprobes and nanocontainers whose characteristics are sensitive to changes in the pH of the medium [5-14]. Thus, in the works [5-9], polymer brushes and layers on various surfaces sensitive to changes in the pH are presented. It has been shown that the density of polymer brushes can be significantly varied [5-8]. This allows for the release of small dye molecules [5] or chromophores [6], the creation of pH-sensitive supramolecular switches [7], and the controlled adsorption of gold nanoparticles bound to the ends of macrochains in a polymer brush [8].

It is known that the intracellular pH in normal cells is in the range of 7.0–7.2 lower than the extracellular pH, which is in the range of 7.3–7.4. Cancer cells have a higher intracellular pH of 7.12–7.65 and lower extracellular pH of 6.2–6.9 compared to normal cells [10–11]. This allows using pH-sensitive conformational

changes in macrochains for cancer diagnostics and therapy. A pH-sensitive nanoprobe was presented in [9], in which the conformational structure of the ligand shell around the quantum dot was reconstructed when the pH level changed from physiological to more acidic, corresponding to a cancer tumor [9]. Photothermal therapy uses gold nanoparticles with a polymer shell, which remain stable in healthy tissue and aggregate when entering a tumor due to changes in pH [12]. Studies [13-14] have examined nanocarriers that are sensitive to changes in pH, such as a gold nanoparticle with a peptide shell containing an anticancer drug. A gold nanoparticle with a polypeptide corona sensitive to pH changes can be used as such a nanosystem. The conformations of polyelectrolyte polypeptides change significantly on the charged surface of the adsorbent [15-21]. By simultaneously varying the charge of the nanoparticle and the degree of polyelectrolyticity of the polypeptide (by changing the pH), it is possible to control the conformational changes of the adsorbed polypeptide.

A more complex picture of conformational rearrangements with changes in pH will arise when several polypeptides are located on the surface of a charged spherical metal nanoparticle. When the pH level changes, two identical polypeptides will be charged with the same sign and magnitude of charge, which will lead to the repulsion of the polypeptides from each other. If the polypeptides in a binary complex consist of amino acid residues of different types, their charge will change differently depending on the values of the isoelectric points characteristic of each polypeptide. Therefore, on the surface of a charged nanoparticle, the conformations of two different polypeptides will change differently depending on the pH level. Such pH-sensitive conformational changes in binary complexes can be used to create small molecule nanocarriers (fluorescent dye molecules or drugs) contained in the structure of the polypeptide fringe and released during its rearrangement when the pH level changes. In addition, such pH-dependent conformations of pairs of macromolecules adsorbed on a charged nanoparticle can be used in SERS, SPR, FRET sensors and nanoprobes.

Thus, the aim of this work is to study the pH-dependent conformations of binary complexes of homogeneous polypeptides on the surface of a charged spherical gold nanoparticle.

2. Mathematical model of macrochain conformations taking into account interactions in a complex of two homogeneous polypeptides on the surface of a charged nanosphere with a change in the hydrogen index of the solvent

In the case where the links of two homogeneous polypeptides at a certain value of the hydrogen index of the solvent acquire charges of opposite sign, a spatial structure with intertwined, oppositely charged macrochains of polyelectrolytes can form on the surface of the charged nanosphere.

2.1 Single adsorbed polyelectrolyte polypeptide chain on the surface of a charged spherical nanoparticle

The description of the equilibrium structure of an adsorbed macrochain with links of length a at an absolute temperature T can be made on the basis of a conformational function $\psi(\mathbf{r})$ satisfying the nonlinear integro-differential equation of Grosberg-Khokhlov-Edwards [22-23]

$$\frac{a^2 kT}{6}\nabla^2\psi(\mathbf{r}) = [V(\mathbf{r}) + V_{self}(\mathbf{r}) - \varepsilon]\psi(\mathbf{r}), \quad (1)$$

The self-consistent field potential $V_{self}(\mathbf{r})$ takes into account the volume interactions between the polymer links. The potential $V(\mathbf{r})$ characterizes the external field in which the polymer chain is located, and which in the case under consideration is created by the adsorbent nanoparticle, electrically neutral or charged.

The spatial distribution of the local density $n(\mathbf{r})$ of chain links is determined by the square of the conformational function $\psi(\mathbf{r})$ corresponding to the minimum eigenvalue ε_0: $n(\mathbf{r}) = \psi^2_{\min}(\mathbf{r})$. In the case of an electrically neutral spherical surface or a nanosphere, the field potential $V(\mathbf{r}) = V_{9-3}(r)$ is the van der Waals interaction potential $V_{9-3}(r)$ of the chain link with the nanoparticle. The exponents 3 and 9 of the power dependences of the potential $V_{9-3}(r)$ on the radius r are typical precisely for the spherical shape of a nanobody. The expression for the potential energy $V(r)$ of interaction of an atom with a nanosphere of radius R can be formed from paired atom-atom potentials of the form $\upsilon(r) = D\left[(r_0/r)^{12} - 2(r_0/r)^6\right]$, and is represented by a

triple integral

$$V(r) = 2\pi \int_0^{\pi} \int_0^{R} n_0 \upsilon(\rho)\, r'^2 dr' \sin\theta d\theta,$$

where $\rho^2 = r'^2 + r^2 - 2rr'\cos\theta$. Here D and r_0 are the parameters of the 6–12 Lennard-Jones potential, n_0 is the concentration of nanosphere atoms. The potential energy of interaction of a chain link with an uncharged spherical nanoparticle of radius R, in the case of the initial pair potential of 6–12 Lennard-Jones for intermolecular interaction between the atoms of the link and the nanoparticle, is written as ($r > R$)

$$V_{9-3}(r) = \frac{\pi D n_0 r_0^6}{6r}\left(\frac{r_0^6}{60}\left[\frac{9R+r}{(R+r)^9} - \frac{9R-r}{(R-r)^9}\right] - \left[\frac{3R+r}{(R+r)^3} - \frac{3R-r}{(R-r)^3}\right]\right). \quad (2)$$

Here D and r_0 are the parameters of the 6-12 Lennard-Jones potential, n_0 is the concentration of metal atoms in the nanoparticle.

In the case of a charged nanoparticle with a spherically symmetrically distributed charge Q and a polyelectrolyte chain with a charge e of its link, the potential $V_{eQ}(r) = eQ/r$ of interaction of the macrochain monomer with the Coulomb field of the charged nanoparticle is added to the adsorption potential (2).

$$V_{9-3}^{eQ}(r) = V_{9-3}(r) + V_{eQ}(r) = V_{9-3}(r) + \frac{eQ}{r}. \quad (3)$$

2.2 Ideal Gaussian macromolecular chain without volume interaction of links

The equilibrium configurations of the macrochain in a model that does not take into account the volume interactions of the links ($V_{self}(\mathbf{r})$=0) are given by the conformational function $\psi_0(\mathbf{r})$, which determines the density of the monomeric subunits of the chain in this approximation as $n(\mathbf{r}) = \psi_0^2(\mathbf{r})$. The function $\psi_0(\mathbf{r})$ then satisfies the following differential equation [22]

$$\frac{a^2 kT}{6}\nabla^2\psi_0(\mathbf{r}) = [V(\mathbf{r}) - \varepsilon]\psi_0(\mathbf{r}). \quad (4)$$

In the case of a polyelectrolyte, it is possible to formulate the problem of determining the conformational structure of the fringe and obtain an exact analytical solution for the conformational function $\psi_0(\mathbf{r})$ satisfying equation (4) without appealing to perturbation theory as in earlier works [19-20]. Equation (4) is similar in certain features to the Schrödinger equation containing the Coulomb potential. In other words, a problem arises similar to the problem of a hydrogen-like atom with an additional potential (2), which, in order to obtain an analytical solution to the problem, is replaced by the model potential "wall – delta-functional well" $V_1(r) = V_\infty(R) - \alpha_0\delta(r - r_0)$ [24]. The total potential $V(r)$ in this case takes the form $V_1(r) = V_\infty(R) - \alpha_0\delta(r - r_0) + eQ/r$, where e is still the effective charge of the chain link, and Q is the charge of the sphere.

We define the following parameters: $q_0^2 = -\frac{6|\varepsilon_0|}{a^2 kT}$, $\kappa = \frac{3eQ}{a^2 kTq_0} = \frac{3eQ}{a\sqrt{6|\varepsilon_0|kT}}$. Instead of the radial function $\psi_0(\mathbf{r}) = F_0(r)$ satisfying equation (4), for a system with spherical symmetry we introduce the function $f(r)$ by the relation $F_0(r) = \exp(-q_0 r) f(r)$, and the dimensionless radius $2q_0 r = \rho'$. By direct substitution into (4) we verify that the function $f(\rho')$ satisfies the degenerate hypergeometric equation

$$\rho' f'' + (\gamma - \rho') f' - \alpha f(\rho') = 0, \quad (5)$$

with γ=2 and $\alpha = 1 - \kappa$. Then the general solution of the boundary value problem for a spherical system with a macromolecular frame is a superposition of two degenerate hypergeometric functions of the first ${}_1F_1(\alpha,\gamma,\rho) \equiv M(\alpha,\gamma,\rho)$ and second $U(\alpha,\gamma,\rho)$ kind with arbitrary constants C_1 and C_2

$$f(\rho) = C_1 M(\alpha,2,\rho) + C_2 U(\alpha,2,\rho), \quad (6)$$

Degenerate hypergeometric functions of the first $M(\alpha,\gamma,\rho)$ and second $U(\alpha,\gamma,\rho)$ kind are defined by the expressions

$$M(\alpha,\gamma,\rho)=\frac{\Gamma(\gamma)2^{1-\gamma}e^{\rho/2}}{\Gamma(\gamma-\alpha)\Gamma(\alpha)}\int_{-1}^{1} e^{-\rho t/2}(1-t)^{\alpha-1}(1+t)^{\gamma-\alpha-1}dt,\ \ \mathrm{Re}\,\gamma>\mathrm{Re}\,\alpha>0, \tag{7}$$

$$U(\alpha,\gamma,\rho)=\frac{1}{\Gamma(\alpha)}\int_{0}^{\infty} e^{-\rho t}t^{\alpha-1}(1+t)^{\gamma-\alpha-1}dt\cdot \tag{8}$$

In radial ranges $2q_0R\le\rho\le 2q_0r_0$ and $2q_0r_0\le\rho$ for functions $f_{I,II}(\rho)$ we can write

$$\begin{cases} f_I(\rho)=C_1M(\alpha,2,\rho)+C_2U(\alpha,2,\rho), & q_0R\le\rho/2\le q_0r_0 \\ f_{II}(\rho)=C_3U(\alpha,2,\rho), & 2q_0r_0\le\rho \end{cases}. \tag{9}$$

$$U(\alpha,2,\rho)=\frac{1}{\Gamma(\alpha-1)}\left[\frac{1}{(\alpha-1)_1\rho}+\sum_{k=0}^{\infty}\frac{(\alpha)_k\rho^k}{k!(2)_k}\left(\ln\rho+\frac{\Gamma'(\alpha+k)}{\Gamma(\alpha+k)}-\frac{\Gamma'(2+k)}{\Gamma(2+k)}-\frac{\Gamma'(1+k)}{\Gamma(1+k)}\right)\right] \tag{10}$$

$$G(\alpha=1-\kappa,n=2,\rho)=\frac{(-1)^n}{(n-1)!\Gamma(\alpha-n+1)}\left\{\sum_{k=1}^{n-1}\frac{(-1)^{k-1}(k-1)!}{(\alpha-k)_k(n-k)_k}\rho^{-k}+\right. \tag{11}$$

$$\left.+\sum_{k=0}^{\infty}\frac{(\alpha)_k}{k!(n)_k}\rho^k\left[\ln\rho+\psi(\alpha+k)-\psi(n+k)-\psi(k+1)\right]\right\},\ (\alpha)_k=\frac{\Gamma(\alpha+k)}{\Gamma(\alpha)},$$

$$\kappa=\frac{3e'Q}{a^2kTq_0}=\frac{3e'Q}{a\sqrt{6\,|\,\varepsilon_0\,|\,kT}}\cdot$$

where Q is the charge of the nanoparticle, and the "energy" parameter $|\,\varepsilon_0\,|=\frac{q^2a^2kT}{6}$.

From the boundary conditions on the surface of the nanoparticle we obtain the following relationships between the constants C_1, C_2 and C_3:

$$C_2=-C_1\frac{M(\alpha,2,2q_0R)}{U(\alpha,2,2q_0R)},$$

$$C_3=C_1\left[\frac{M(\alpha,2,2q_0r_0)}{U(\alpha,2,2q_0r_0)}-\frac{M(\alpha,2,2q_0R)}{U(\alpha,2,2q_0R)}\right]. \tag{12}$$

Then the desired solutions of the Grosberg-Khokhlov equation take the form

$$\begin{cases} F_I(r)=C_1\left[M(\alpha,2,2q_0r)-\frac{M(\alpha,2,2q_0R)}{U(\alpha,2,2q_0R)}U(\alpha,2,2q_0r)\right]\exp\left(-q_0r\right), & R\le r\le r_0 \\ F_{II}(\rho)=C_1\left[\frac{M(\alpha,2,2q_0r_0)}{U(\alpha,2,2q_0r_0)}-\frac{M(\alpha,2,2q_0R)}{U(\alpha,2,2q_0R)}\right]U(\alpha,2,2q_0r)\exp\left(-q_0r\right), & r_0\le r \end{cases} \tag{13}$$

To determine the parameters q_l and ε_l it is necessary to solve the equation obtained for the jump in the radial derivative at the point r_0

$$F'_{II0}(r)\,|_{r=r_0+0}-F'_{I0}(r)\,|_{r=r_0-0}=-\frac{6\alpha_0}{a^2kT}F_{I0}(r_0) \tag{14}$$

Substituting (13) into (14) we obtain the general transcendental equation for the eigenvalues

$$\frac{3\alpha_0}{a^2\alpha kTq_0}-\left[\frac{U(\alpha+1,3,2q_0r_0)}{U(\alpha,2,2q_0r_0)}\right]= \tag{15}$$

$$=\left[\frac{M(\alpha+1,3,2q_0r_0)}{2U(\alpha,2,2q_0r_0)}+\frac{M(\alpha,2,2q_0R)}{U(\alpha,2,2q_0R)}\frac{U(\alpha+1,3,2q_0r_0)}{U(\alpha,2,2q_0r_0)}\right]\left[\frac{M(\alpha,2,2q_0r_0)}{U(\alpha,2,2q_0r_0)}-\frac{M(\alpha,2,2q_0R)}{U(\alpha,2,2q_0R)}\right]^{-1}$$

It should be noted that the degenerate hypergeometric functions (7) and (8) in a number of cases, with a certain relationship between the parameters α and γ, are expressed through the Bessel functions of the

imaginary argument

$$I_\nu(\rho)=\frac{(\rho/2)^\nu}{\Gamma(\nu+1)}\exp(-\rho)M(\nu+1/2,2\nu+1,2\rho), \tag{16}$$

$$K_\nu(\rho)=\sqrt{\pi}(2\rho)^\nu\exp(-\rho)U(\nu+1/2,2\nu+1,2\rho). \tag{17}$$

Since γ=2 and $\alpha=1-\kappa$, $\kappa=\frac{3e'Q}{a^2kTq_0}=\frac{3e'Q}{a\sqrt{6|\varepsilon_0|kT}}$, to obtain γ=2 it is necessary that γ=2=$(2\nu+1)$, whence it follows that $\nu=1/2$. This means that $\alpha=1$ and Q=0. Thus, in this case we obtain an electrically neutral nanoparticle, and the same, uncharged, macrochain. Formulas (13) go over to the previously obtained expressions with Bessel functions $I_{1/2}$, $K_{1/2}$.

In this case, for a spherically symmetric potential $V_1(r)=V_\infty(R)-\alpha_0\delta(r-r_0)$, the radial functions $\psi(\mathbf{r})=F_0^{I,II}(r)$ are defined inside the spherical layer $R<r<r_0$ and in the region conjugate to it $r>r_0$ in the following form

$$\begin{cases} F_0^I(r)=A_0\left[\dfrac{I_{1/2}(q_0r)}{\sqrt{r}}-\dfrac{I_{1/2}(q_0R)}{K_{1/2}(q_0R)}\dfrac{K_{1/2}(q_0r)}{\sqrt{r}}\right], & R<r<r_0 \\ F_0^{II}(r)=A_0\left[\dfrac{I_{1/2}(q_0r_0)}{K_{1/2}(q_0r_0)}-\dfrac{I_{1/2}(q_0R)}{K_{1/2}(q_0R)}\right]\dfrac{K_{1/2}(q_0r)}{\sqrt{r}}, & r_0<r<\infty \end{cases}, \tag{18}$$

where $I_{1/2}(q_0r)$ and $K_{1/2}(q_0r)$ are modified Bessel functions of the first and second kind with half-integer index, and eigenvalues $q_0^2=-\frac{6\varepsilon_0}{a^2kT}$, R is the radius of the nanoparticle. The transcendental equation (14) for the eigenvalue q_0 is transformed to the equation

$$\frac{a^2kT}{6\alpha r_0}=I_{1/2}(q_0r_0)K_{1/2}(q_0r_0)-K_{1/2}^2(q_0r_0)\frac{I_{1/2}(q_0R)}{K_{1/2}(q_0R)}, \tag{19}$$

which is related to (15), but allows us to define in a new way q_0, and with it the only discrete level of the spectrum ε_0. The conformational characteristics (18) of the chain in the case of an uncharged nanoparticle or an electrically neutral macromolecule are indifferent to changes in the charge states of the system components.

Thus, for the case of a polyelectrolyte fringe adsorbed by a charged nanosphere, neglecting volume interactions, we have an exact analytical solution to the problem presented by formulas (13) and (15). Note that, unlike the aligned polyampholyte links of a macrochain, for which there was always an attraction to the surface, regardless of the sign of the nanoparticle charge, in the case of a polyelectrolyte chain under consideration, there may be both an additional attraction (opposite signs of the charges of the link and the particle) against the background of the attractive potential responsible for the adsorption of the macromolecule, and a repulsion (identical signs of the charges), which hinders adsorption or even leads to desorption at a sufficiently high temperature of the system. This additional Coulomb attraction or repulsion of the links to the surface of the nanoparticle will ultimately determine the observed compression or loosening of the reinforced fringe of the adsorbate.

Quantitatively, this is reflected in the sign of the charge parameter $\alpha-1=\pm|\kappa|$. With the same signs of the charge of the links and the adsorbent, under the conditions of realized adsorption of the macrochain, swelling of the fringe will be observed, caused by the Coulomb repulsion from the surface of the links that have avoided attraction by the potential well. For the same reason, in the case of opposite charges, the macrochain fringe should experience Coulomb compression

$$\alpha=1\pm|\kappa|.$$

In order to develop an analytical model convenient for carrying out calculations, potential $V_{9-3}(r)$ (2) can be replaced by a simple model potential $V_{\alpha\delta}^\infty(r)=V_\infty(R)-\alpha_0\delta(r-r_0)$ "solid wall – delta-functional well", in which the point r_0 of localization of the delta-functional well coincides with the radius r_m of the bottom of the potential well (2).

2.3 Accounting for volumetric interlink interactions of a polymer chain

The bulk interlink interactions of the polymer can be taken into account through the potential $V_{self}(\mathbf{r})$ of the self-consistent field using the Edwards method [23]

$$V_{self}(\mathbf{r}) = \mu^*\left(n(\mathbf{r})\right) = kT \cdot B \cdot n(\mathbf{r}), \tag{20}$$

where $\mu^*\left(n(\mathbf{r})\right)$ is the chemical potential of the chain links:

$$B(T) = \frac{2\pi}{3}\left(\frac{\beta'}{T}\right)^{1/4}\Gamma\left(3/4\right),$$

– the second virial coefficient [22], taking into account pairwise collisions of links and the effect of excluded volume due to the repulsive part of the 6–12 Lennard-Jones potential, and the constant

$$\beta' = \left[\beta \pm (Q \cdot e \cdot r_D^{11})\exp(-r/r_D)|_{r\to r_D}\right] \tag{21}$$

renormalized taking into account the additional charge on the links of the macrochain and the Debye screening with radius r_D. The gamma function Γ of ¾ takes the numerical value

$$\Gamma\left(3/4\right) = \sqrt{2\pi^2}/\Gamma(1/4), \quad \Gamma(1/4) = 2\sqrt{K(1/2)\sqrt{\pi}} \approx 3{,}626.$$

In the case of Coulomb interaction of polyelectrolyte units with each other, one can introduce the corresponding pair potential $\Phi_{qq}(r)$, and represent the renormalized constant β' in the form

$$\beta \to \beta' = \left[\left(D + \Phi_{qq}(r_0)\right)\cdot r_0^{12}\right]. \tag{22}$$

Then the model potential in the Grosberg-Khokhlov-Edwards equation (1) can be written as

$$V(r) + V_{self}(\mathbf{r}) = V_\infty(R) - \alpha_0\delta(r - r_0) + kT \cdot B \cdot n(\mathbf{r}).$$

Let us write equation (1) for the conformational function $\psi_1(\mathbf{r})$ of the first macrochain

$$\frac{a_1^2 kT}{6}\nabla^2\psi_1(r) = \left[V_{9-3}^{(1)}(r) + kTB_1n_1(r) + e_1\varphi_2(r) + \frac{e_1Q}{r} - \varepsilon_1\right]\psi_1(r). \tag{23}$$

Here, in (23), the electrostatic field potential $\varphi_2(r)$ is created by the charged chain 2 of the second polyelectrolyte and affects the formation of the secondary structure of chain 1 through its conformational function $\psi_1(\mathbf{r})$. It is also obvious that the potential $\varphi_2(r)$ satisfies the Poisson equation

$$\frac{1}{r^2}\frac{d}{dr}r^2\frac{d}{dr}\varphi_2(r) = -4\pi e_2\psi_2^2(r). \tag{24}$$

Equations similar to (23) and (24) can be written by considering the conformations of chain 2 in the field of the charged chain 1. Then, for the conformational functions $\psi_{1,2}(\mathbf{r})$ and potentials $\varphi_{1,2}(r)$, we obtain a closed system of nonlinear differential equations.

2.4 Formation of conformations of two interacting adsorbed polyelectrolyte chains on the surface of a charged nanosphere

Combining all the equations considered into a system, we obtain four interconnected ordinary differential equations

$$\begin{cases} \dfrac{a_1^2kT}{6}\dfrac{1}{r^2}\dfrac{d}{dr}r^2\dfrac{d}{dr}\psi_1(r) = \left[V_{9-3}^{(1)}(r) + kT \cdot B_1\psi_1^2(r) + e_1\varphi_2(r) + \dfrac{e_1Q}{r} - \varepsilon_1\right]\psi_1(r) \\ \dfrac{a_2^2kT}{6}\dfrac{1}{r^2}\dfrac{d}{dr}r2\dfrac{d}{dr}\psi_2(r) = \left[V_{9-3}^{(2)}(r) + kT \cdot B_2\psi_2^2(r) + e_2\varphi_1(r) + \dfrac{e_2Q}{r} - \varepsilon_2\right]\psi_2(r) \\ \dfrac{1}{r^2}\dfrac{d}{dr}r^2\dfrac{d}{dr}\varphi_1(r) = -4\pi e_1\psi_1^2(r) \\ \dfrac{1}{r^2}\dfrac{d}{dr}r^2\dfrac{d}{dr}\varphi_2(r) = -4\pi e_2\psi_2^2(r) \end{cases}. \tag{25}$$

The self-consistent system of equations (25) for conformational functions $\psi_{1,2}(\mathbf{r})$ and potentials $\varphi_{1,2}(r)$ is quite complex, and obtaining analytical expressions for functions $\psi_{1,2}(\mathbf{r})$ and $\varphi_{1,2}(r)$ is problematic. However, the general structure of the model based on system (25) is partially visible even without resorting to exact solutions of these equations. In addition, sufficient progress in solving the problem can be made by adopting the approximation of relatively weak electrolyte fields. Then, in the zero approximation, the potentials $\varphi_{1,2}(r)$ are not taken into account in the first two equations of system (25), and the conformational functions $\psi_{1,2}(\mathbf{r})$ in this approximation are found as $\psi_{1,2}(\mathbf{r}) \to \psi_{1,2}^{(0)}(\mathbf{r})$.

$$\begin{cases} \dfrac{a_1^2 kT}{6}\dfrac{1}{r^2}\dfrac{d}{dr}r^2\dfrac{d}{dr}\psi_1^{(0)}(r) = \left[V_{9-3}^{(1)}(r) + kT\cdot B_1\psi_1^{(0)2}(r) + \dfrac{e_1 Q}{r} - \varepsilon_1\right]\psi_1^{(0)}(r) \\ \dfrac{a_2^2 kT}{6}\dfrac{1}{r^2}\dfrac{d}{dr}r^2\dfrac{d}{dr}\psi_2^{(0)}(r) = \left[V_{9-3}^{(2)}(r) + kT\cdot B_2\psi_2^{(0)2}(r) + \dfrac{e_2 Q}{r} - \varepsilon_2\right]\psi_2^{(0)}(r) \\ \dfrac{1}{r^2}\dfrac{d}{dr}r^2\dfrac{d}{dr}\varphi_1^{(0)}(r) = -4\pi e_1\psi_1^{(0)2}(r) \\ \dfrac{1}{r^2}\dfrac{d}{dr}r^2\dfrac{d}{dr}\varphi_2^{(0)}(r) = -4\pi e_2\psi_2^{(0)2}(r) \end{cases}. \quad (26)$$

In this case, the last two equations in (26) – the Poisson equations, become autonomous and can be solved by standard electrostatic methods for a given charge distribution density $e_{1,2}\left[\psi_{1,2}^{(0)}(r)\right]^2$ if the solutions $\psi_{1,2}^{(0)}(\mathbf{r})$ of the first two equations of system (26) are found beforehand. After this, the found potentials $\varphi_{1,2}^{(0)}(r)$ of the zero approximation are returned to system (25) to find the functions $\psi_{1,2}^{(1)}(\mathbf{r})$ and potentials $\varphi_{1,2}^{(1)}(r)$ of the first approximation. To achieve the required level of accuracy, this iterative procedure can be continued.

As in Section 2.2, to find in analytical form the radial distribution of links of a polymer chain adsorbed by a charged nanoparticle of radius *R*, the potential energy (2) of the interaction of an atom with a nanosphere should be replaced by a simple model potential $V_{\alpha\delta}^{\infty}(r) + \dfrac{e_{1,2}Q}{r} = V_{\infty}(R) - \alpha\delta(r - r_m) + \dfrac{e_{1,2}Q}{r}$ "solid wall – delta-functional well".

The solutions $\psi_{1,2}^{(0)}(r)$ of equations (26) without taking into account the effects of the self-consistent field are then written in the form (13), where the parameters $q_{1,2}^2 = -\dfrac{6\varepsilon_{1,2}}{a_{1,2}^2 kT}$ are the roots of two transcendental equations of type (15).

The only roots of these equations correspond to functions $\psi_{1,2}^{(0)}(r)$ whose squares give the desired expressions for the radial distributions $n_{1,2}^{(0)}(r) = \psi_{1,2}^{(0)2}(r)$ of the density of links of chains 1 and 2.

2.5 Calculation of field potentials and interaction energy of adsorbed polyelectrolyte chains

The Green's function of the two Laplace equations in (26) of the external Dirichlet problem ($r>R$) for a ball has the form

$$G(r,\theta,\phi;r_0,\theta_0,\phi_0) = \frac{1}{4\pi}\left(\frac{1}{r_{MM_0}} - \frac{R}{r_0\cdot r_{MM_1}}\right). \quad (27)$$

The point M_1 is the conjugate point of M_0 relative to the surface of the sphere. Then the zeroth approximation potentials $\varphi_{1,2}^{(0)}(r)$ outside the sphere ($r>R$) can be written in quadratures

$$\varphi_{1,2}(r) = \int_0^{\pi} \sin\theta_0 d\theta_0 \int_R^{\infty} e_{1,2}\psi_{1,2}^{(0)2}(r_0)G(r,\theta,\phi;r_0,\theta_0,\phi_0)2\pi r_0^2 dr_0 \cdot \quad (28)$$

The interaction energy of chains in some cases may be of independent interest and is determined by integrals

$$W[n_1(r),n_2(r)] = \int_R^{\infty} e_1 n_1(r)\varphi_2(r)4\pi r^2 dr = \int_R^{\infty} e_2 n_2(r)\varphi_1(r)4\pi r^2 dr \quad . \quad (29)$$

3. Molecular dynamics simulation

Molecular dynamics (MD) simulations were performed for polypeptides on the surface of a gold nanoparticle with a radius of about 3 nm [25]. MD simulations were performed using the NAMD 2.14 software package [26]. A number of combinations of polypeptides, each 100 units long, were considered:

1) one macromolecule of histidine His amino acid residues,

2) two macromolecules of histidine amino acid residues – the **HH** polypeptide complex,

3) one polypeptide of histidine His units, and the other of glutamic acid Glu units – the **HG** polypeptide complex.

The following pH range was chosen: from 4 to 7.6. At pH≈4, all polyhistidine units have a positive charge, and at the isoelectric point for histidine pI_{His}≈7.6, all units become uncharged His^0. As the pH increases in this range, some amino acid residues change their charge and become neutral [27]. A number of macrochains with different charged units were considered:

1) polypeptide His_{100} (total charge of the macrochain +100*e*) - corresponds to a hydrogen index level of pH≈4;

2) polypeptide $(His_2His^0His)_{25}$ (total charge +75*e*) - pH≈5.5;

3) polypeptide $(His^0His)_{50}$ (total charge +50*e*) - pH≈6;

4) polypeptide $(His^0{}_2HisHis^0)_{25}$ (total charge +25*e*) - pH≈6.5;

5) polypeptide $(His^0{}_5HisHis^0{}_4)_{10}$ (total charge +10*e*) – pH≈7;

6) polypeptide $His^0{}_{100}$ (uncharged macromolecule) at isoelectric point pI_{His}≈7.6.

For polypeptides, the CHARMM36 force field was used [28–29]. The interaction with the gold nanoparticle was described by the Lennard-Jones potential [30]. Long-range electrostatic interactions were calculated using the particle–mesh Ewald (PME) method [31]. The entire system was contained in a cube with 25 nm edges containing TIP3P water molecules [32]. MD simulations were initially performed at a constant temperature of 600 K and at 300 K in the final portion of the trajectory. This allowed us to reach deeper minima in the macrochain's conformational energy, including over a shorter trajectory. To monitor the attainment of equilibrium conformations, we monitored the change in the root-mean-square distance (RMSD) between polypeptide atoms in different conformations. The simulation time reached 30 ns with a step size of 1 fs. Three different starting conformations were considered for each combination of macrochains.

Initially, the polymers were located near a neutral gold nanoparticle. In this case, a single polyhistidine or a pair of polyhistidines in the HH complex in the starting conformation were at the isoelectric point. As a result of the simulation, adsorption of a single polyhistidine (Fig. 1a) and two polyhistidines (Fig. 5a) on the surface of an uncharged gold nanoparticle was observed. The obtained equilibrium structures of polypeptides at the isoelectric point were subsequently used as starting points in modeling with a lower pH value.

The macrochains in the HG complex at the initial moment of time were at a hydrogen index value of pH≈5.5, that is, when most of the polyhistidine units were positively charged, and the polyglutamate units were negatively charged by approximately 90 percent - $(Glu_5Glu^0Glu_4)_{10}$ (the parameters of which were set in the same way as in [33]). Therefore, a polymer complex of two oppositely charged macromolecules of polyhistidine and polyglutamate (Fig. 7a), intertwined with each other, was formed on the surface of the nanoparticle. Subsequently, during modeling for this nanosystem, the pH level increased, and the hydrogen index values were taken in the range from 6 to 8, in which all polyglutamate units were negatively charged. The following values of the surface charge density of the nanoparticle were considered: ±σ, ±2σ, ±5σ, ±10σ, ±20σ, where σ≈0.2*e*/nm^2, 2σ≈0.4*e*/nm^2, 5σ≈1*e*/nm^2, 10σ≈2*e*/nm^2, 20σ≈4*e*/nm^2 (the partial charge of the atom on the surface is ±0.01*e*, ±0.02*e*, ±0.05*e*, ±0.1*e*, and ±0.2*e*, respectively [34]).

4. Results

4.1 Conformations of a single homogeneous polypeptide on a charged gold nanoparticle with changing pH

Molecular dynamics simulations of single polyhistidine at an isoelectric point of pI_{His}≈7.6 revealed polymer adsorption on the nanoparticle (Fig. 1a). As the pH value varied, the rigidity of the polyelectrolyte macrochain increased. At a low polyelectrolytic level, the adsorption pattern was similar to that observed at the isoelectric point. If the degree of polyelectrolyticity was high, then the macrochain initially compactly adsorbed on the surface of the nanoparticle began to unfold with the release of loops into the surrounding space (Fig. 1c). This type of adsorption is typical of highly charged polyelectrolytes [35]. Figure 2a shows that the strongest decrease in the density of polymer atoms is observed at the lowest pH≈4 value considered.

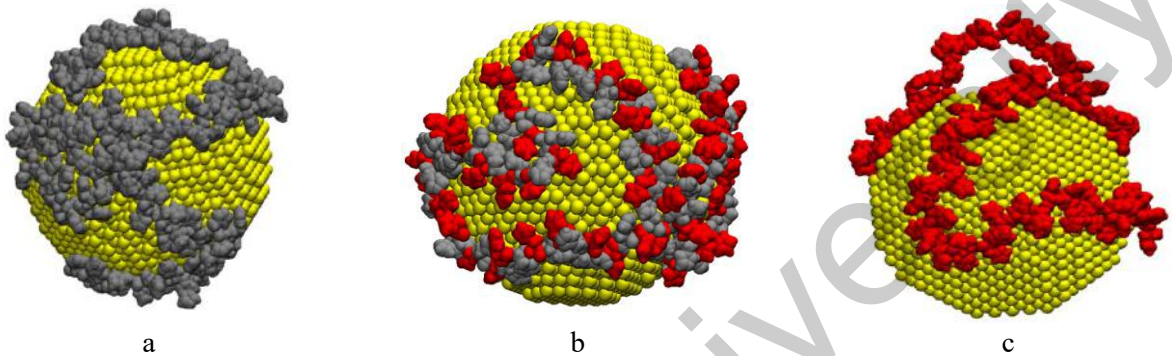

a b c

Fig. 1. Single polyhistidine on the surface of an uncharged gold nanoparticle after simulation at the isoelectric point pI_{His}≈7.6 (a), as well as at pH≈6 (b) and pH≈4 (c). Uncharged amino acid residues His0 are shown in gray, and positively charged His are shown in red.

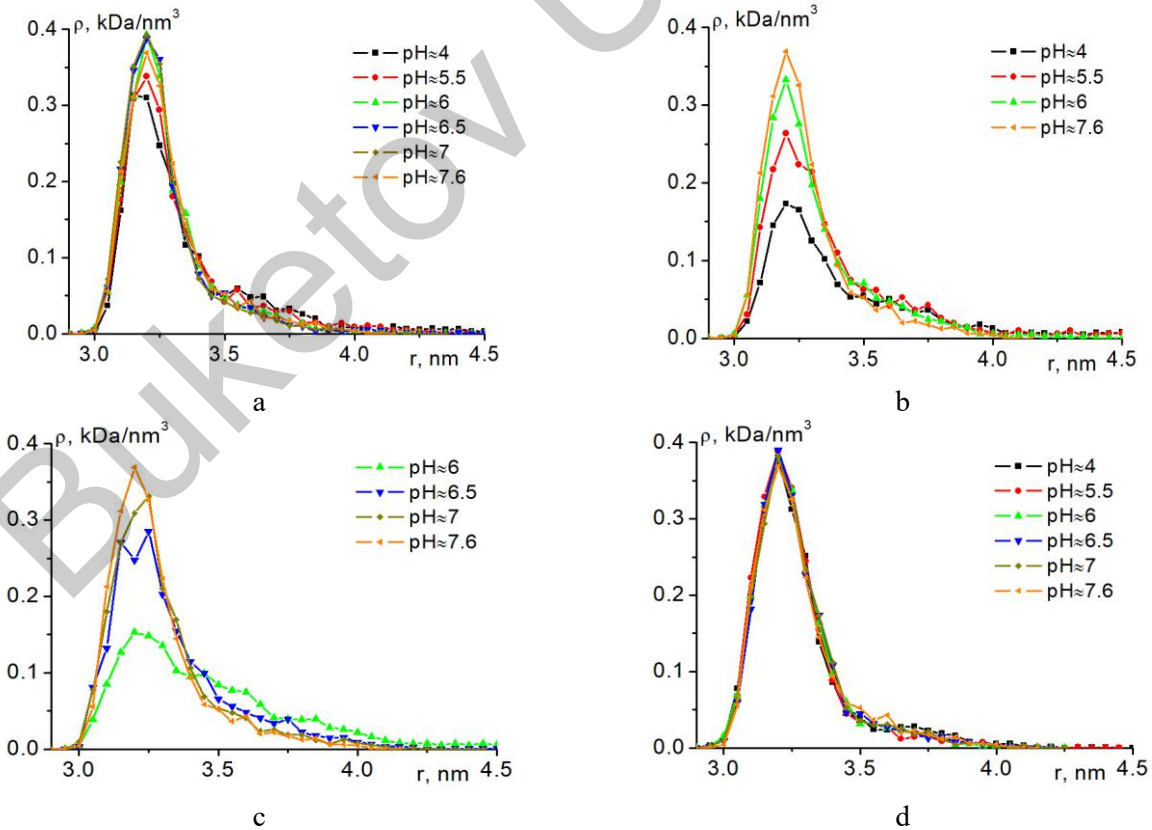

a b

c d

Fig. 2. Radial dependences of the average atomic density of a single polyhistidine on an uncharged gold nanoparticle (a), as well as on a charged gold nanoparticle with a surface density of +2σ (b), +5σ (c), and -5σ (d) at different pH levels.

If the nanoparticle was negatively charged, the positively charged polyhistidine units were attracted to the surface of the nanoparticle. This was most pronounced when the degree of polyelectrolyticity of the polypeptide was high. The swollen polyelectrolyte fringe at pH≈4 on an uncharged nanoparticle (Fig. 1c) was compressed on a negatively charged surface (Fig. 3a). When the nanoparticle was positively charged, the charged polyhistidine units were repelled from the like-charged surface. This led to the macromolecular corona first swelling, followed by polyelectrolyte desorption.

Figure 3b shows that at a surface charge density of +5σ and a pH of ≈6, desorption of a significant polymer fragment is observed. When the pH level was equal to pH≈4 and pH≈5.5, polyelectrolyte desorption occurred at a surface charge density of +5σ, while at pH≈6 the polypeptide desorbed at +10σ, and at pH≈6.5 – at +20σ. At pH≈7, macrochain desorption did not occur; however, the polyelectrolyte flake swelled significantly at +20σ compared to the neutral surface of the nanoparticle, when the polypeptide conformation was similar to the polypeptide conformation at the isoelectric point. Figures 2b and 2c show that, for the same nanoparticle charge, the density of polypeptide atoms near the nanoparticle surface varies significantly at different pH values. The lower the pH, the more severe the loosening of the macrochain fringe on the positively charged surface (Figures 2b and 2c). When the nanoparticle was negatively charged (Figure 2d), the radial atom density distribution curves were very close to each other due to the fact that the positively charged macrochain was adsorbed on the nanoparticle.

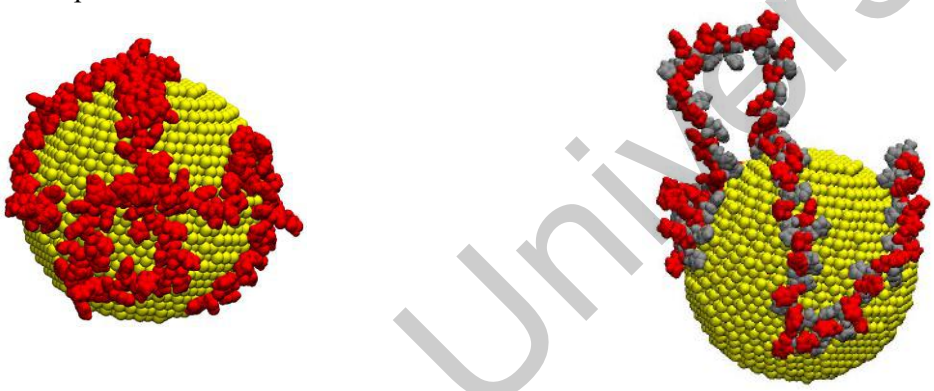

a b

Fig. 3. Single polyhistidine after simulation on the surface of a gold nanoparticle charged with a surface charge density of -5σ at pH≈4 (a), and at pH≈6 and +5σ (b). Uncharged amino acid residues His0 are shown in gray, and positively charged His are shown in red.

Figure 4 shows that for polypeptides with varying degrees of polyelectrolyticity, the conformational structure of the macromolecular corona around the nanosphere changes from dense to swollen over different ranges of surface charge density.

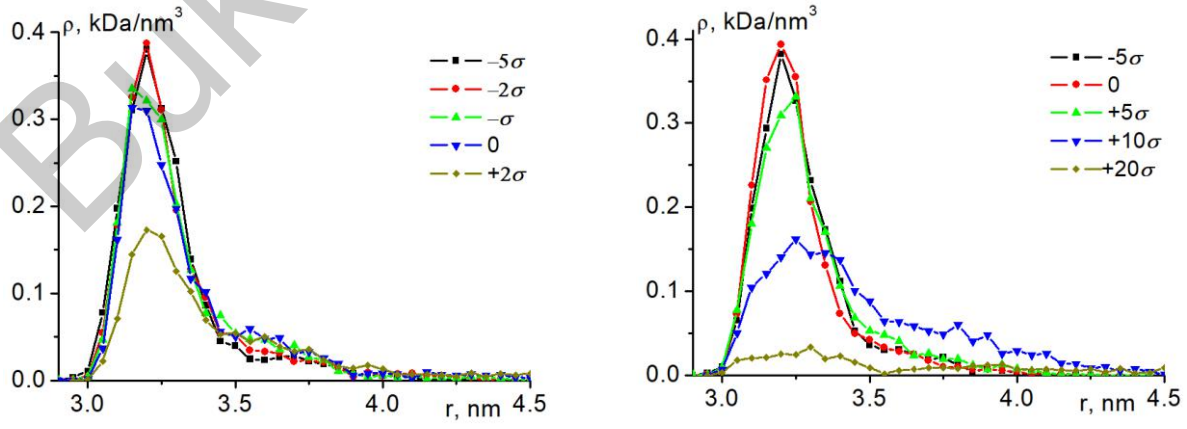

a b

Fig. 4. Radial dependences of the average atomic density of adsorbed single polyhistidine at different surface charge densities of gold nanoparticles at pH≈4 (a) and pH≈7 (b).

For a highly charged polymer molecule (Fig. 4a, pH ≈ 4), the polymer layer begins to swell at a surface charge density of -σ, i.e., with a charge opposite to that of the macrochain. For a polyelectrolyte with a low degree of polyelectrolyticity (Fig. 4b, pH≈7), swelling of the macrochain fringe begins to occur only at a surface charge density of the nanoparticle of +5σ, at which polyhistidine at pH≈4 has already desorbed.

4.2 Conformations of two identical polypeptides on a charged gold nanoparticle with changing pH

In the case of MD simulation, at the isoelectric point of two identical polypeptides on a spherical gold nanoparticle, both macrochains were adsorbed on its surface, partially intertwined with each other (Fig. 5a). As the pH level decreased, the macromolecules began to repel each other, as they became equally charged. With a small degree of polyelectrolyticity of polypeptides, the forces of electrostatic repulsion between the macrochains were insufficient to overcome the van der Waals forces and shift them from each other by a significant distance, therefore, the polypeptide fragments moved only slightly from each other. With a further decrease in the pH level and, accordingly, an increase in the degree of polyelectrolyticity, the polypeptides shift to different sides of the gold nanoparticle, repelling each other (Fig. 5b).

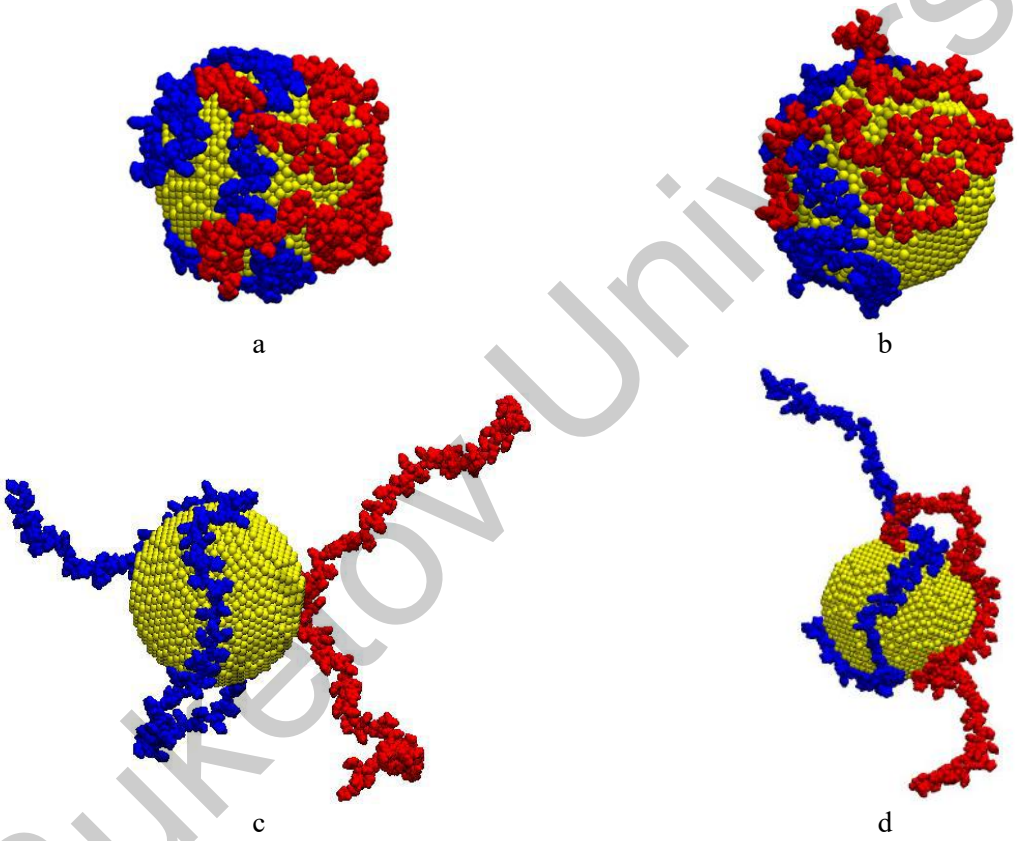

Fig. 5. Two macromolecules of histidine units (HH polypeptide complex) on the surface of a neutral gold nanoparticle after simulation: at the isoelectric point pI_{His}≈7.6 (a) and at pH≈4 (b), as well as on a nanoparticle charged with a surface density of -5σ at pH≈4 (c) and +5σ at pH≈6 (d). The first and second polypeptides are shown in red and blue, respectively.

Figure 6a shows that with decreasing pH and increasing the degree of polyelectrolyticity of the macrochains, there is a significant decrease in the concentration of units near the surface of the nanosphere. At pH≈4, the peak distribution for two macrochains decreased by approximately 30 percent compared to the peak of this distribution at the isoelectric point (Fig. 6a). This decrease is much greater than for a single polypeptide, where the peak distribution of polyelectrolyte atoms at pH≈4 decreased by approximately 13 percent compared to the peak distribution at the isoelectric point (Fig. 2a). This indicates a stronger swelling of the polymer layer with increasing polyelectrolyticity of two polyhistidines compared to a single macromolecule due to the electrostatic repulsion between similarly charged polypeptides.

Adsorption of positive polypeptide units in the HH binary complex occurred on the surface of a highly negatively charged nanoparticle (-5σ and below) at low pH. The loose polymer fringe on the neutral nanoparticle (Fig. 5b, pH≈4) contracted and tightly enveloped the oppositely charged nanoparticle (Fig. 5c, pH≈4). Figure 6b shows the combined distributions of two polyhistidine macromolecules on a charged nanoparticle with a surface density of -5σ. It can be seen that the distribution curves for the HH polypeptide complex with varying degrees of polyelectrolyte (pH≤7) are very close to those for their adsorption at the isoelectric point pI_{His}≈7.6.

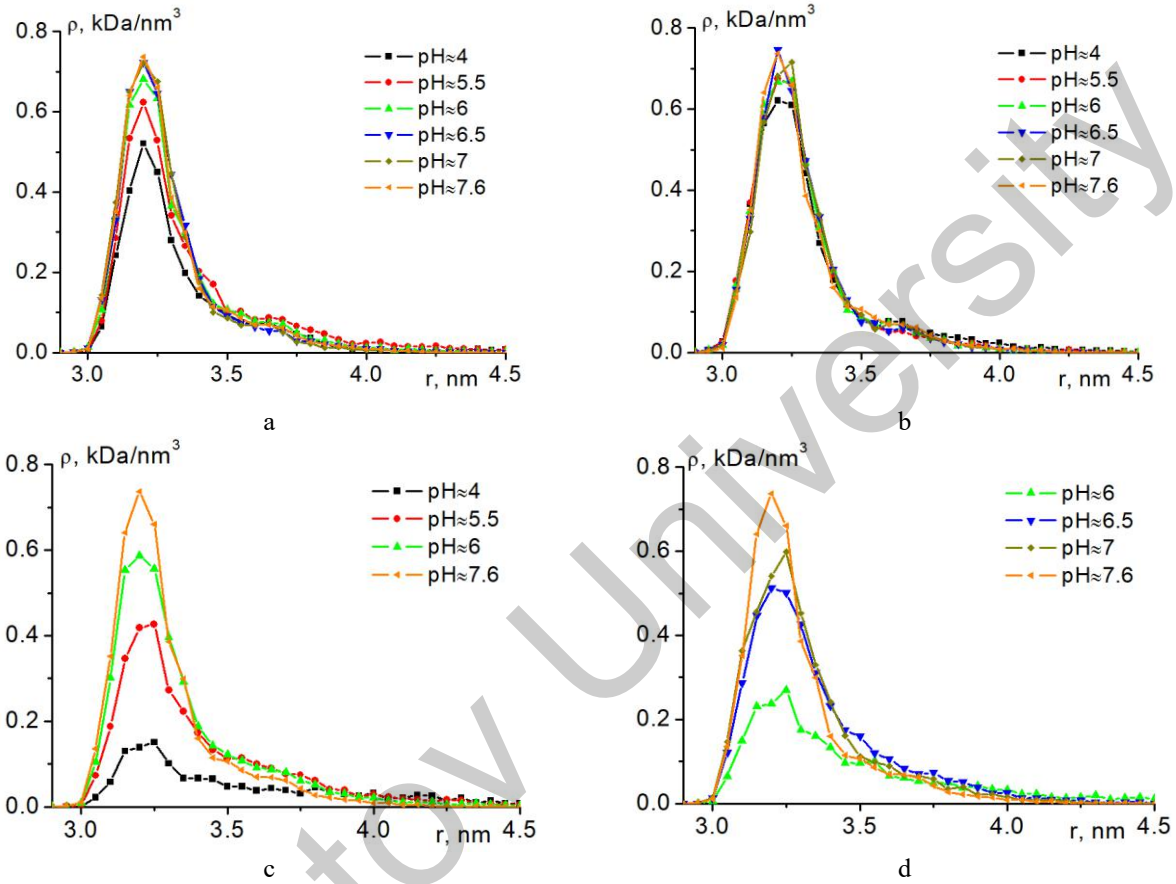

Fig. 6. Total radial dependences of the average density of atoms of two polyhistidine macromolecules on an uncharged (a) and charged gold nanoparticle with a surface density of -5σ (b), +2σ (c), and +5σ (d) at different pH levels.

As the nanoparticle charge increased, the polyelectrolyte fringe first swelled (Fig. 5d, +5σ at pH≈6), and then the macromolecules desorbed. The sparsity of the polyelectrolyte fringe of two polyhistidines around the gold nanoparticle at the same surface charge density depended significantly on the pH. Figures 6c and 6d show that at lower pH, the distributions for the HH polypeptide complex are significantly lower at the same charge, indicating significant swelling of the polyelectrolyte fringe. The lower the degree of polyelectrolyticity of the polypeptides in the HH complex, the higher the nanoparticle charge value at which desorption of macromolecules was observed: at pH≈4 and pH≈5.5 - at a surface charge density equal to +5σ, at pH≈6 - at +10σ, at pH≈6.5 - at +20σ, and at pH≈7 no desorption was observed, as in the case of single polyglutamate.

4.3 Conformations of a binary polyhistidine-polyglutamate complex on a charged gold nanoparticle with varying pH

At pH ≈ 5.5, polyhistidine and polyglutamate in the HG complex were oppositely charged and attracted to each other, intertwining (Fig. 7a). As pH increased, the charge of polyhistidine gradually decreased and became zero at the isoelectric point pI_{His}≈ 7.6, while the absolute charge of polyglutamate reached its maximum at pH≈6 and remained unchanged. The electrostatic attraction between the macrochains decreased with increasing pH, while the interunit repulsion in polyglutamate increased. Therefore, polyglutamate was released from its bond with polyhistidine and unfolded, releasing fragments into the space surrounding the nanoparticle (Fig. 7b). Meanwhile, polyhistidine remained folded on the surface of the gold nanoparticle.

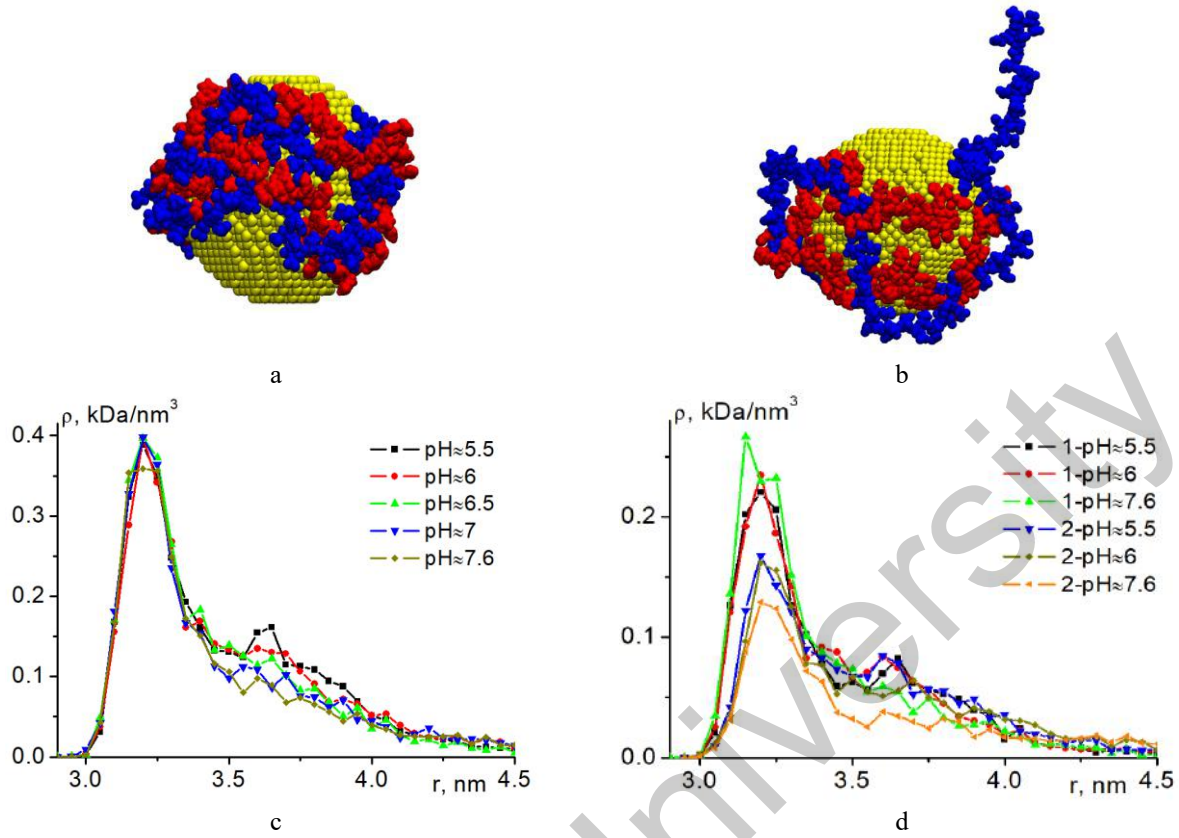

Fig. 7. Macromolecules of polyhistidine (red) and polyglutamate (blue) after simulation on the surface of an uncharged gold nanoparticle at pH≈5.5 (a) and pH≈7.6 (b). Total radial dependences of the average density of polypeptide atoms in the HG complex (c), as well as radial dependences of the average density of polyhistidine (d, curves 1) and polyglutamate (d, curves 2) atoms in the HG complex separately on the surface of an uncharged gold nanoparticle at different pH levels.

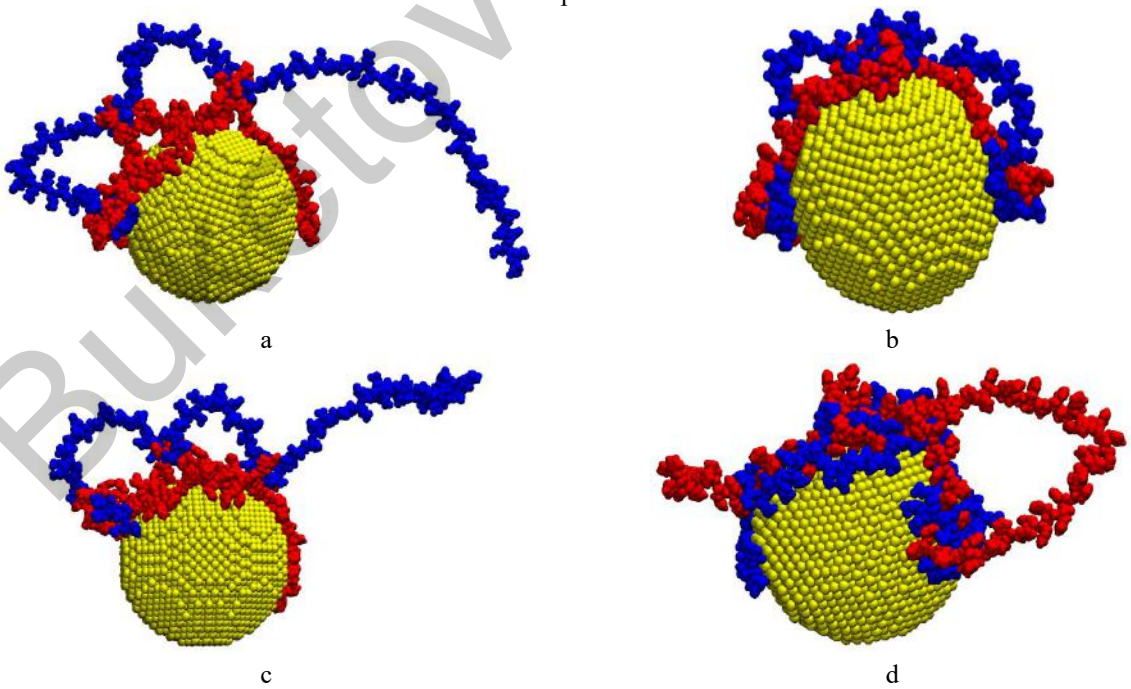

Fig. 8. Macromolecules of polyhistidine (red) and polyglutamate (blue) after simulation on the surface of a gold nanoparticle charged with a surface density of -5σ at pH≈7.6 (a) and pH≈6 (b), at -10σ and pH≈6 (c), at +10σ and pH≈5.5 (d).

Figure 7c shows the total distributions of polyhistidine and polyglutamate atoms in the HG complex at different pH levels on the surface of a neutral nanoparticle. It is clear that as the pH increases, the distribution curves become very close to each other, decreasing slightly at pH ≈ 7.6, when polyglutamate is maximally released from its bond with polyhistidine. A different picture is observed for the distributions of polyhistidine and polyglutamate atoms in the HG complex, constructed separately for each polypeptide (Fig. 7d). With increasing pH, the distributions for polyhistidine and polyglutamate behave differently: the curves for polyglutamate decrease, while the peak values of the distribution for polyhistidine increase (Fig. 7d).

The decrease in the concentration of polyglutamate atoms near the surface of the nanoobject is associated with the unfolding of the polymer with increasing pH (Fig. 7b). And the increase in the concentration of polyhistidine atoms near the surface is associated with the substitution of desorbed polyglutamate units (Fig. 7b). At pH≈7.6, polyhistidine was uncharged at the isoelectric point, so on the negatively charged surface of the nanoparticle, the negatively charged polyglutamate was repelled from the nanoparticle, and the polymer corona swelled. At a surface charge density of -5σ, polyglutamate was almost completely desorbed, retaining itself in the HG complex due to entanglement with polyhistidine and pulling its loops into the surrounding space (Fig. 8a). On a positively charged nanoparticle at pH≈7.6, the fringe swollen due to the unfolding of polyglutamate (Fig. 7b) was compressed due to the electrostatic attraction of the negatively charged polyglutamate to the surface. On a positively charged nanoparticle, a mirror image was observed when the pH level was reduced. The lower the pH level, the greater the degree of polyelectrolyticity of polyhistidine, and it was increasingly repelled from the surface of the nanoparticle (Fig. 8d). And polyglutamate, on the contrary, was increasingly attracted to the positively charged surface. A polymer fringe was formed, in which polyglutamate was concentrated at the surface, and polyhistidine was at the periphery. Thus, the structure and swelling character of the fringe from the HG polypeptide complex changed significantly with changes in both the surface charge and the pH level. Figure 9a shows the total distributions for the HG complex depending on the charge density on the nanoparticle surface at pH≈5.5.

It is evident that with an increase in the absolute value of the nanosphere charge, the total density of polypeptide atoms decreases. This is due to the swelling of the polypeptide fringe of two oppositely charged macrochains, since the macrochain charged like the nanoparticle shifts to the periphery. Therefore, the curves of the radial dependences of the average density of polyhistidine (Fig. 9b) and polyglutamate (Fig. 9c) atoms behave differently with a change in the nanoparticle charge at pH≈5.5. For polyhistidine (Fig. 9b), the atomic density at the surface of a negatively charged nanoparticle slightly increases compared to a neutral nanoparticle, while it decreases significantly on a positively charged surface. In this case, the density of polyglutamate atoms changes in a mirror image when the charge of the nanoparticle changes (Fig. 9c). And at pH≈7.6, when polyhistidine becomes neutral, the negatively charged polyglutamate macrochain is repelled from the surface (Fig. 8a), so the density of polyglutamate atoms at the surface of a negatively charged nanoparticle decreases significantly (Fig. 9d). Figure 10 shows the radial dependences of the average density of polyglutamate atoms at different pH levels at -5σ (Fig. 10a) and +5σ (Fig. 10b). It is evident (Fig. 10a) that with increasing pH, the number of polyglutamate atoms near the surface decreases significantly due to the release of polyglutamate from adhesion to neutralizing polyhistidine and the repulsion of polyglutamate from the surface. On a positively charged nanosphere (Fig. 10b), with increasing pH, the density of polyglutamate atoms increases slightly due to displacement toward the surface after release from polyhistidine.

4.4 Results of calculations based on the mathematical model

To compare the calculation results based on the analytical model with the MD simulation data, Fig. 11 a, b, c shows the graphs of the radial dependences of the conformational functions $\psi(r) \equiv F(r) = F_0^{I,II}(r)$ for different signs of the charge parameter $\alpha = 1 - \kappa$, $\kappa = \pm|\kappa|$. Curves 1 in all three Figures 11 a, b, c correspond to the same signs of the charges of the spherical nanoparticle and the polymer chain links: $qQ>0$, therefore the maxima of the curves $\psi(r) \equiv F(r) = F_0^{I,II}(r)$ at the points r_0 of the minimum potential are located below the maxima of curves 2, which are calculated for the case of qQ<0, i.e., with the appearance of additional attraction of the charged chain links to the nanoparticle surface. Curves 1 are characterized by a more gradual attenuation in the asymptotics, as should be the case of swelling of the polymer corona.

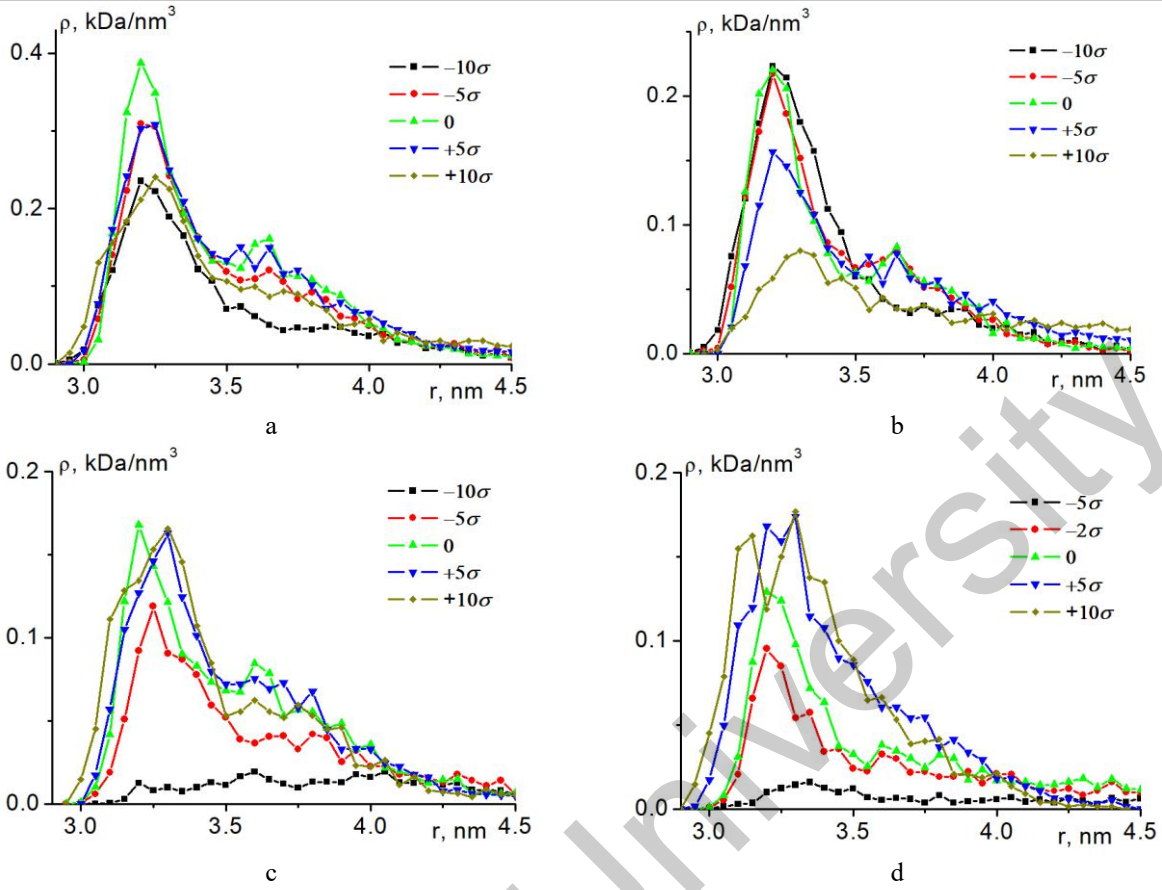

Fig. 9. Total radial dependences of the average density of polypeptide atoms in the HG complex (a), as well as radial dependences of the average density of polyhistidine (b) and polyglutamate (c) atoms in the HG complex separately at different surface charge densities of the gold nanoparticle at pH≈5.5, as well as radial dependences of the average density of polyglutamate atoms at pH≈7.6 (d).

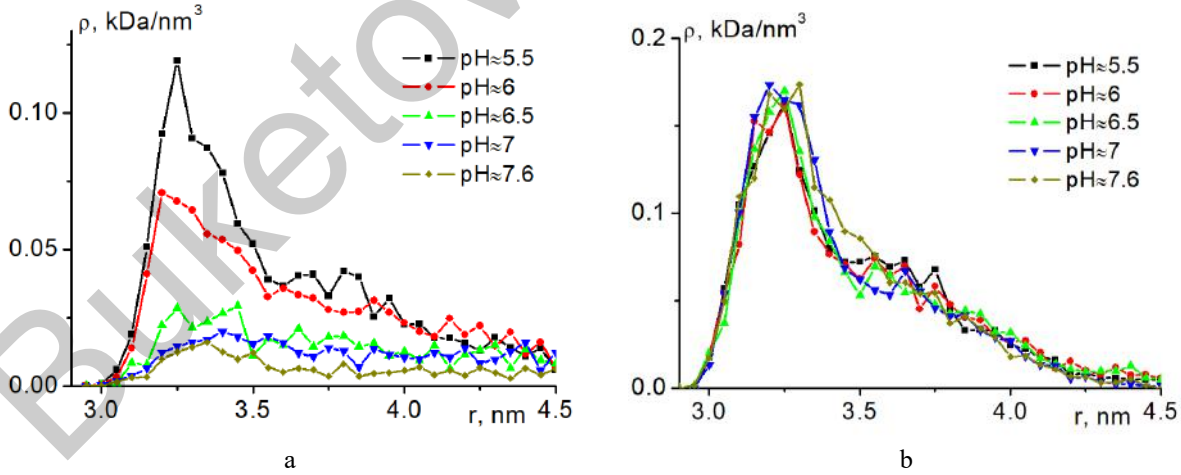

Fig. 10. Radial dependences of the average density of polyglutamate atoms at different pH levels with a surface charge density of gold nanoparticles of -5σ (a) and +5σ (b).

For large values of the charge parameter modulus $|\kappa|=\frac{3|qQ|}{a^2kTq_0}$ – 0.9 for Fig. 11a versus 0.2 for Fig. 11b and 0.1 for Fig. 11c, curves 1 and 2 exhibit a larger amplitude of divergence of the function F with changes in the radial variable in Fig. 11a compared to Fig. 11b and Fig. 11c. That is, for uncharged nanoparticles or electrically neutral polymer chains, curves 1 and 2 coincide. To cover a wider range of values, the radial variable of the function F is expressed in dimensionless rq units.

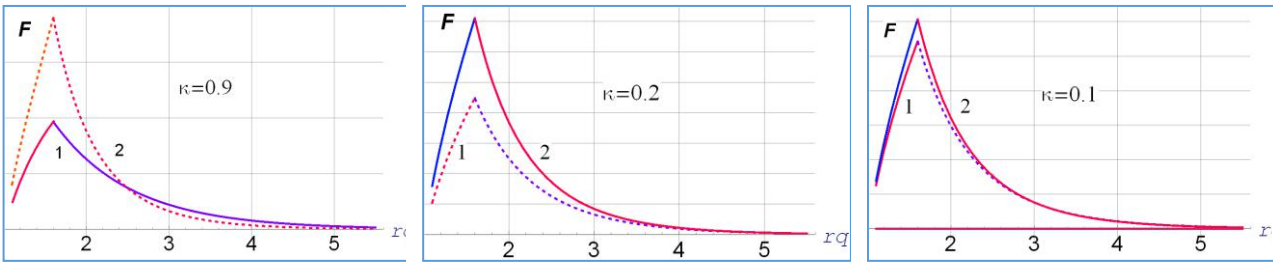

a b c

Fig. 11. Radial dependences of conformational functions for different signs of the charge parameter: 1– $qQ>0$, 2– $qQ<0$ and three values of its modulus: 0.9 (a), 0.2 (b) and 0.1 (c).

Thus, the theoretical model proposed in this paper qualitatively accurately conveys the observed features of the interaction of two polyelectrolyte chains with a charged nanoparticle, revealed by MD simulations with specific adsorbed polypeptides upon changes in the solution pH and the nanoparticle charge.

5. Conclusion

The conformations of homogeneous polypeptides adsorbed on the surface of a charged spherical gold nanoparticle are significantly restructured with changes in the pH level and charge of the nanoparticle, and in the case of adsorption of two polypeptides on a nanoparticle, the structure of the macromolecular fringe depends significantly on the combinations in which the polypeptides are found in the binary complex.

A single homogeneous polypeptide adsorbed on a neutral gold nanoparticle unfolds from a tangled ball structure when the pH level deviates from the isoelectric point, and the polymer fringe around the nanoparticle begins to swell. On an oppositely charged nanoparticle, the swollen polyelectrolyte fringe contracts, while on the surface of a similarly charged nanoparticle it swells (up to desorption) as the pH level deviates from the isoelectric point.

Two identical homogeneous polypeptides adsorbed on an uncharged gold nanoparticle begin to repel and shift from each other along the surface when the pH value deviates from the isoelectric point. Since the size of the nanoparticle is much smaller than the length of the macrochain, the desorption of polypeptide fragments in the binary complex begins at a lower degree of polyelectrolyticity of the macromolecules and the rarefaction of the peptide layer on the surface of the neutral nanoparticle was stronger than for a single macrochain at the same deviation of the pH level from the isoelectric point.

On the surface of a neutral gold nanoparticle, oppositely charged macrochains were tightly intertwined. On the charged nanoparticle, the macromolecule with the same charge as the nanoparticle shifted to the periphery, while the oppositely charged polyelectrolyte remained near the surface. This created two layers of different types of polypeptides within the polymer crown, which swelled significantly. Upon reaching the isoelectric point of one of the polypeptides, the charge of the second polypeptide became uncompensated. Therefore, the second charged polypeptide began to unfold and disengage from the first uncharged macromolecule. On the nanoparticle, which was oppositely charged relative to the second polypeptide, the macromolecular crown contracted. And if the nanoparticle was charged in the same way as the second polypeptide, then it shifted to the outer side of the polymer fringe and could desorb faster, the higher the absolute value of the nanoparticle charge was, and the pH level was closer to the isoelectric point of the first polypeptide.

To describe the conformations of adsorbed charged macrochains, a mathematical model based on a closed self-consistent system of equations for conformational functions $\psi_{1,2}(\mathbf{r})$ and electrostatic potentials $\varphi_{1,2}(r)$ is proposed. To take into account the volume interactions of chain links, self-consistent field potentials were introduced into the model using the Edwards method. Obtaining solutions to the closed system of differential equations is based on an iterative procedure. The proposed model qualitatively correctly conveys the observed features of the interaction of two polyelectrolyte chains, revealed as a result of MD simulation with specific adsorbed polypeptides with changes in pH and nanoparticle charge.

Thus, such changes in polypeptide conformations can be used to create pH-sensitive nanoprobes, nanocontainers, and elements of various biochemical sensors. If small functional molecules are introduced into

the polypeptide edging, then when the pH level changes with a change in the conformations of the polypeptides, a shift of the introduced small molecules relative to the surface of the nanoparticle or their release from the polymer edging will occur. This nanosystem can be used as a pH-sensitive container for targeted delivery of drugs with their controlled release at the final destination. If molecules of organic dyes are included in the polymer edging, then the pH-sensitive change in the distance between them, as well as the change in the distance between the dyes and the plasmonic nanoparticle, can be used as a method for controlling the efficiency of the luminescent signal of this hybrid nanosystem, since the various channels of deactivation of the electronic excitation of photoactive molecules depend significantly on the spatial arrangement of the molecules relative to the plasmonic nanoparticle.

Conflict of interest statement

The authors declare that they have no conflict of interest in relation to this research, whether financial, personal, authorship or otherwise, that could affect the research and its results presented in this paper.

CRediT author statement

Kruchinin N.Yu.: Conceptualization, Methodology, Software, Investigation, Writing - Original Draft; **Kucherenko M.G.**: Conceptualization, Methodology, Investigation, Writing - Original Draft.
The final manuscript was read and approved by all authors.

Acknowledgements

This work was supported by the Ministry of Science and Higher Education of the Russian Federation within the framework of project no. FSGU-2023-0003

References

1 Kanp T., Dhuri A.M., Rode K., Aalhate M., Paul P., Nair R., Singh P.K. (2025) Exploring the potential of nanocarriers for cancer immunotherapy: insights into mechanism, nanocarriers, and regulatory perspectives. *ACS Appl. Bio Mater*., 8, 108–138. https://doi.org/10.1021/acsabm.4c01797

2 Mi S., Hu X., Yuan S., Yu H., Guo Y., Cheng Y., Yao W. (2024) Unveiling the correlation between protein, protein corona, and target signal loss in SERS detection. *Anal. Chem.,* 96, 19768–19777. https://doi.org/10.1021/acs.analchem.4c05084

3 Gao J., Yang W., Liu R., Feng, J., Li Y., Jiang M., Jiang, S. (2024) A reliable gold nanoparticle/Cu-TCPP 2D MOF/gold/D-shaped fiber sensor based on SPR and LSPR coupling for dopamine detection. *Applied Surface Science,* 655, 159523. https://doi.org/10.1016/j.apsusc.2024.159523

4 Liu M., Zhuang H., Zhang Y., Jia Y. (2024) A sandwich FRET biosensor for lysozyme detection based on peptide-functionalized gold nanoparticles and FAM-labeled aptamer. *Talanta,* 276, 126226. https://doi.org/10.1016/j.talanta.2024.126226

5 Kumar S., Dory Y.L., Lepage M., Zhao Y. (2011) Surface-grafted stimuli-responsive block copolymer brushes for the thermo-, photo- and pH-sensitive release of dye molecules. *Macromolecules,* 44, 7385–7393. https://doi.org/10.1021/ma2010102

6 Cui J., Nguyen T., Ceolín M., Berger R., Azzaroni O., del Campo A. (2012) Phototunable response in caged polymer brushes. *Macromolecules,* 45, 3213–3220. https://doi.org/10.1021/ma300274b

7 Jacquelín D.K., Perez M.A., Euti E.M., Arisnabarreta N., Cometto F.P., Paredes-Olivera, P., Patrito E.M. (2016) A pH-Sensitive supramolecular switch based on mixed carboxylic acid terminated self-assembled monolayers on Au(111). *Langmuir*, 32, 947–953. https://doi.org/10.1021/acs.langmuir.5b03807

8 Filip J., Popelka A., Bertok T., Holazova A., Osicka J., Kollar J., Ilcikova M., Tkac J., Kasak P. (2017) pH-Switchable Interaction of a carboxybetaine ester-based SAM with DNA and gold nanoparticles. *Langmuir,* 33, 6657–6666. https://doi.org/10.1021/acs.langmuir.7b00568

9 Debayle M., Marchandier T., Xu X., Lequeux N., Pons T. (2019) pH-Sensitive visible or shortwave infrared quantum dot nanoprobes using conformation-switchable copolymeric ligands. *ACS Appl. Mater. Interfaces,* 11, 25008–25016. https://doi.org/10.1021/acsami.9b06194

10 Shirmanova M.V., Druzhkova I.N., Lukina M.M., Matlashov M.E., Belousov, V.V., Snopova L.B., Prodanetz N.N., Dudenkova V.V., Lukyanov S.A., Zagaynova E.V. (2015) Intracellular pH imaging in cancer cells in vitro and tumors in vivo using the new genetically encoded sensor SypHer2. *Biochimica et Biophysica Acta (BBA) - General Subjects*, 1850, 1905-1911. https://doi.org/10.1016/j.bbagen.2015.05.001

11 Webb B., Chimenti M., Jacobson M.P., Barber D.L. (2011) Dysregulated pH: a perfect storm for cancer progression. *Nature Reviews Cancer,* 11, 671–677. https://doi.org/10.1038/nrc3110

12 Liu X., Chen Y., Li H., Huang N., Jin Q., Ren K., Ji J. (2013) Enhanced retention and cellular uptake of nanoparticles in tumors by controlling their aggregation behavior. *ACS Nano* 7, 6244–6257. https://doi.org/10.1021/nn402201w

13 Chen W., Lei Q., Luo G., Jia H., Hong S., Liu Y., Cheng Y., Zhang X. (2015) Rational Design of Multifunctional Gold Nanoparticles via Host−Guest Interaction for Cancer-Targeted Therapy. *ACS Appl. Mater. Interfaces,* 7, 17171–17180. https://doi.org/10.1021/acsami.5b04031

14 Yari-Ilkhchi A., Rafi A.A., Mahkam M. (2025) Design and development of pH-sensitive nanocarriers using molecularly imprinted polymers for the targeted delivery of sodium thiopental. *Nanoscale Advances,* 7, 2039-2046. https://doi.org/10.1039/d4na00926f

15 Kruchinin N.Yu., Kucherenko M.G. (2021) Rearrangements in the conformational structure of polyampholytic polypeptides on the surface of a uniformly charged and polarized nanowire: Molecular dynamics simulation. *Surfaces and Interfaces,* 27, 101517, https://doi.org/10.1016/j.surfin.2021.101517

16 Kruchinin N.Yu., Kucherenko M.G. (2022) Molecular dynamics simulation of the conformational structure of uniform polypeptides on the surface of a polarized metal prolate nanospheroid with varying pH. *Russian Journal of Physical Chemistry A*, 96, 624–632. https://doi.org/10.1134/S0036024422030141

17 Kruchinin N.Yu., Kucherenko M.G. (2022) Conformational Changes in Polyampholyte Macrochains on the Surface of an Oblate Metallic Nanospheroid in Alternating Electric Field. *High Energy Chemistry*, 56, 499-510. https://doi.org/10.1134/S0018143922060108

18 Kruchinin N.Yu. (2023) Rearrangement of the conformations of polyampholitic macromolecules on the surface of a charged spherical metal nanoparticle in an alternating electric field: molecular dynamic simulation. *Russian Journal of Physical Chemistry A,* 97, 2777–2785. https://doi.org/10.1134/S003602442312018X

19 Kruchinin N.Yu., Kucherenko M.G. (2024) Conformational structure of a complex of two oppositely charged polyelectrolytes on the surface of a charged spherical metal nanoparticle. *High Energy Chemistry,* 58, 615–623. https://doi.org/10.1134/S0018143924700590

20 Kucherenko M.G., Kruchinin N.Yu., Neyasov P.P. (2024) Conformational structure of polyampholytes and polyelectrolytes on the surface of a longitudinally polarized gold spherocylinder. *Eurasian Physical Technical Journal* 21 (3), 6-20. https://doi.org/10.31489/2024No3/6-20

21 Kruchinin N.Yu., Kucherenko M.G. (2025) Conformational changes of two oppositely charged poly-electrolytes, including those combined into a single block copolymer, on the surface of a charged or transversely polarized cylindrical metal nanowire. *Journal of Polymer Research,* 32,79. https://doi.org/10.1007/s10965-025-04305-3

22 Grosberg A.Y., Khokhlov A.R. (1994) Statistical Physics of Macromolecules. AIP Press, New York. 347.

23 Edvards S.F. (1965) The statistical mechanics of polymers with excluded volume. *Proc. Phys. Soc*., 85, 613-624. https://doi.org/10.1088/0370-1328/85/4/301

24 Kucherenko M.G., Rusinov A.P., Chmereva T.M., Ignat'ev A.A., Kislov D.A., Kruchinin N.Yu. (2009) Kinetics of photoreactions in a regular porous nanostructure with cylindrical cells filled with activator-containing macromolecules. *Optics and Spectroscopy* ,107, 480–485. https://doi.org/10.1134/S0030400X0909029X

25 Mhashal A.R., Roy S. (2014) Effect of Gold Nanoparticle on Structure and Fluidity of Lipid Membrane. *PLoS One* 9, e114152. https://doi.org/10.1371/journal.pone.0114152

26 Phillips J.C., Braun R., Wang W., Gumbart J., Tajkhorshid E., Villa E., Chipot C., Skeel R.D., Kale L., Schulten K. (2005) Scalable molecular dynamics with NAMD. *J. Comput. Chem.,* 26, 1781-1802. https://doi.org/10.1002/jcc.20289

27 Batys P., Morga M., Bonarek P., Sammalkorpi M. (2020) pH-Induced Changes in Polypeptide Conformation: Force-Field Comparison with Experimental Validation. *J. Phys. Chem. B,* 124, 2961-2972. https://doi.org/10.1021/acs.jpcb.0c01475

28 MacKerell Jr. A.D., Bashford D., Bellott, M., Dunbrack Jr. R.L., Evanseck J.D., Field M.J., Fischer S., Gao J., Guo H., Ha S., Joseph-McCarthy D., Kuchnir L., Kuczera K., Lau F.T.K., Mattos C., Michnick S., Ngo T., Nguyen D.T., Prodhom B., Reiher III W.E., Roux B., Schlenkrich M., Smith J.C., Stote R., Straub J., Watanabe M., Wiorkiewicz-Kuczera J., Yin D., Karplus M. (1998) All-Atom Empirical Potential for Molecular Modeling and Dynamics Studies of Proteins. *J. Phys. Chem. B,* 102, 3586-3616. https://doi.org/10.1021/jp973084f

29 Huang J., Rauscher S., Nawrocki G., Ran T, Feig M., de Groot B.L., Grubmüller H., MacKerell Jr. A.D. (2016) CHARMM36m: an improved force field for folded and intrinsically disordered proteins. *Nature Methods,* 14, 71-73. https://doi.org/10.1038/nmeth.4067

30 Heinz H., Vaia R.A., Farmer B.L., Naik R.R. (2008) Accurate simulation of surfaces and interfaces of face-centered cubic metals using 12−6 and 9−6 Lennard-Jones potentials. *J. Phys. Chem. C,* 112, 17281-17290. https://doi.org/10.1021/jp801931d

31 Darden T., York D., Pedersen L. (1993) Particle mesh Ewald: An N·log(N) method for Ewald sums in large systems. *J. Chem. Phys.* 98, 10089-10092. https://doi.org/10.1063/1.464397

32 Jorgensen W.L., Chandrasekhar J., Madura J.D., Impey R.W., Klein M.L. (1983) Comparison of simple potential functions for simulating liquid water. *J. Chem. Phys.*, 79, 926-935. https://doi.org/10.1063/1.445869

33 Radak B.K., Chipot C., Suh D., Jo S., Jiang W., Phillips J.C., Schulten K., Roux. B. (2017) Constant-pH Molecular Dynamics Simulations for Large Biomolecular Systems. *J. Chem. Theory Comput*., 13, 5933-5944. https://doi.org/10.1021/acs.jctc.7b00875

34 Chen P., Zhang Z., Gu N., Ji M. (2018) Effect of the surface charge density of nanoparticles on their translocation across pulmonary surfactant monolayer: a molecular dynamics simulation. *Molecular Simulation*, 44, 85-93. https://doi.org/10.1080/08927022.2017.1342118

35 Harvey J.D., Baker H.A., Mercer E., Budhathoki-Uprety J., Heller D.A. (2017) Control of Carbon Nanotube Solvatochromic Response to Chemotherapeutic Agents. *ACS Appl. Mater. Interface*s, 9, 37947–37953. https://doi.org/10.1021/acsami.7b12015

AUTHORS' INFORMATION

Kruchinin, Nikita Yurievich – Doctor of Physical and Mathematical Sciences, Associate Professor, Associate Professor of the Department of Radio physics and Electronics of the Orenburg State University, Orenburg, Russia; SCOPUS Author ID 35170029600; https://orcid.org/0000-0002-7960-3482; kruchinin_56@mail.ru

Kucherenko, Michael Gennadievich – Doctor of Physical and Mathematical Sciences, Professor, Director of the Center for Laser and Information Biophysics at Orenburg State University, Orenburg, Russia; SCOPUS Author ID 700358146; https://orcid.org/0000-0001-8821-2427; clibph@yandex.ru